Computers and Geotechnics 102 (2018) 125–135

Contents lists available at ScienceDirect

Computers and Geotechnics

journal homepage: www.elsevier.com/locate/compgeo

Research Paper

Unified modeling of soil behaviors before/after flow liquefaction

Ye Bin[a,b,*], Ni Xueqian[a], Huang Yu[a], Zhang Feng[c]

[a] Department of Geotechnical Engineering, College of Civil Engineering, Tongji University, Shanghai 200092, China
[b] State Key Laboratory of Geohazard Prevention and Geoenvironment Protection, Chengdu 610059, China
[c] Graduate School of Engineering, Nagoya Institute of Technology, Nagoya 4668555, Japan

ARTICLE INFO

Keywords:
Soil liquefaction
Flow liquefaction
Constitutive model
Elastoplasticity
Phase transition
Cyclic mobility

ABSTRACT

Flow liquefaction of soil involves a phase transition process from solid to fluid. A constitutive model that can describe the soil behaviors of both the solid and fluid phases in a unified way was proposed. The constitutive model adopts a phase transition criterion to detect the onset of flow liquefaction and associates an elastoplastic relation and a fluid relation in a single framework. The simulated results demonstrated that the proposed model can describe the fundamental behaviors of soil in both the solid and fluid phases with a smooth transition from soil-like behavior to fluid-like behavior during the phase transition process.

1. Introduction

Soil liquefaction is one of the most dangerous threats to civil engineering structures constructed in sandy grounds when earthquakes occur, as evidenced by the 1964 Niigata earthquake in Japan [1], the 1976 Tangshan earthquake in China [2], the 1995 Hyogoken-Nambu earthquake in Japan [3], and the 2008 Wenchuan earthquake in China [4]. Liquefaction-induced ground failure can cause many kinds of geo-disasters and structural damage, such as the settlement of buildings, the uplift of underground facilities, the lateral flow of ground, and even landslides. Therefore, scholars and engineers have devoted great effort to investigating the behaviors and mechanisms of soil liquefaction.

Generally, soil liquefaction behaviors can be divided into two types: cyclic mobility and flow liquefaction [5–7]. Cyclic mobility often occurs in medium-dense sand as a result of the stepwise increase in the pore water pressure and is in connection with repeated contractive and dilative responses when the effective stress approaches a zero state (Fig. 1(a)). Flow liquefaction often occurs in loose sand due to a rapid drop in shear strength and is mainly associated with a contractive response of the soil (Fig. 1(b)). Both types of liquefaction behaviors have been theoretically modeled over the past several decades. For cyclic mobility, liquefaction-induced deformation is generally finite and thus can be described by elastoplastic constitutive models established based on the principles of solid mechanics [8–13]. For flow liquefaction, however, the behavior is more complex because it involves a process in which the soil will transit from a solid phase into a fluid phase and finally result in a very large flow deformation [14]. Because liquefied soil behaves similar to a fluid after liquefaction, the post-liquefaction behavior is no longer suitable to be described by traditional elastoplastic constitutive models. In recent years, some researchers began to adopt fluid dynamics methods to study the flow process of liquefied soil. In their studies, the liquefied soil is regarded as a fluid and thus its behavior can be modeled by a fluid constitutive model. Uzuoka et al. [15] made the first attempt to use a fluid constitutive model (Bingham model) to describe the large deformation caused by flow liquefaction. Chen et al. [16] found that the post-liquefaction behavior of sand can be well simulated by non-Newtonian fluid models. Moriguchi [17] used a CIP-based fluid dynamics method to describe the large deformation of geomaterials in liquefied state. Huang et al. [18] introduced the Bingham fluid model with the Mohr-Coulomb yield criterion into the smoothed particle hydrodynamics (SPH) framework to analyze the flow process of liquefied soil. Zhou et al. [19] proposed a fluid constitutive model for liquefied sand, in which the friction resistance and viscous resistance were expressed as a thixotropic shear-thinning fluid and a non-time-variant shear-thinning fluid, respectively. Although researchers have obtained many results by using the fluid constitutive model to simulate the post-liquefaction behaviors of soil, there is a limitation in these studies that only the fluid-like behavior after liquefaction can be simulated, and the solid-like behavior before liquefaction and the transition process from the solid phase to a fluid phase are omitted. Certainly, it is practicable to use an elastoplastic model to simulate the solid-like behavior before liquefaction, and then use a fluid constitutive model to simulate the fluid-like behavior after liquefaction. However, the method used to separate the pre- and post-liquefaction behaviors is not suitable for the analysis of the entire process from solid behavior to post-liquefaction flow behavior. Particularly, the transition

* Corresponding author at: Department of Geotechnical Engineering, College of Civil Engineering, Tongji University, Shanghai 200092, China.
E-mail address: yebinmail1977@gmail.com (B. Ye).

https://doi.org/10.1016/j.compgeo.2018.06.011
Received 15 March 2018; Received in revised form 5 May 2018; Accepted 13 June 2018

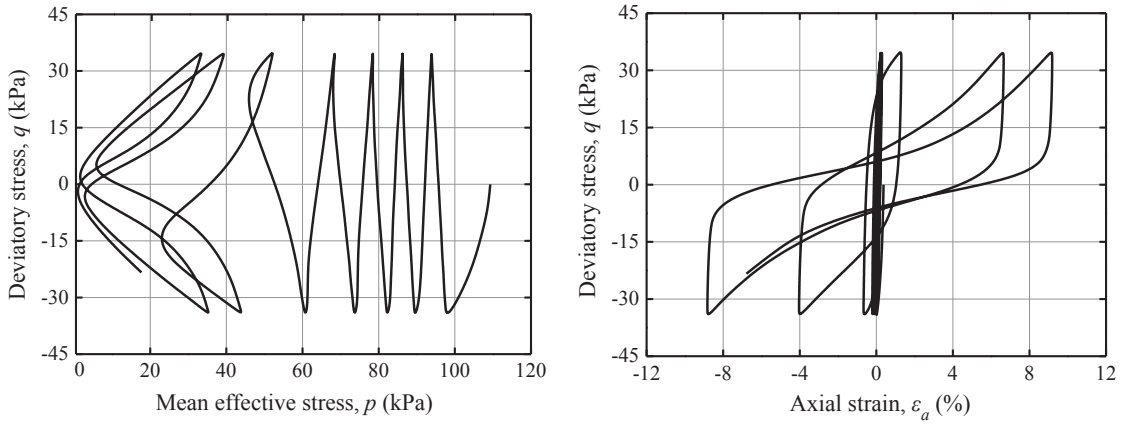

(a) Cyclic mobility (medium-dense sand, D_r=44%)

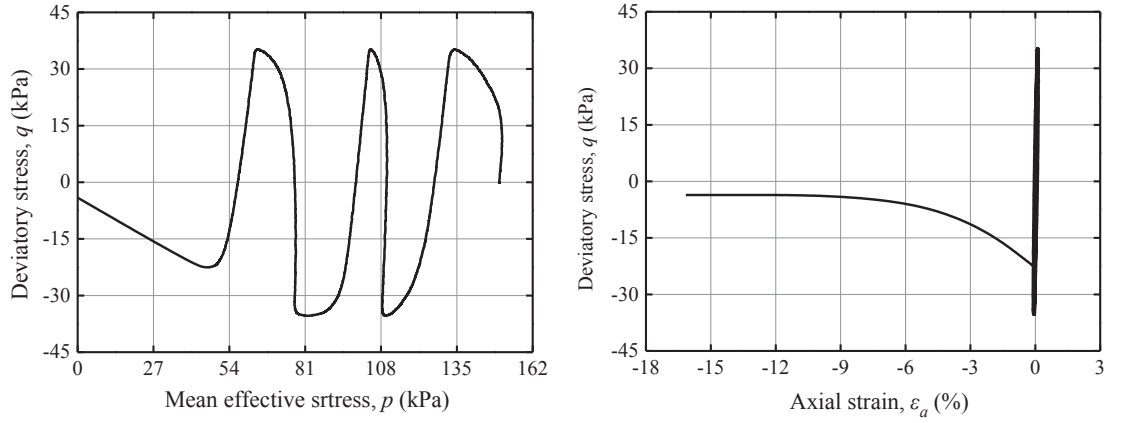

(b) Flow liquefaction (loose sand, D_r=10%)

Fig. 1. Cyclic triaxial tests on medium-dense and loose Fujian sand under an undrained condition.

process from a solid phase to a fluid phase cannot be properly described. In many cases, researchers and engineers expect to understand and predict the entire process of flow liquefaction from the initial solid state to the final fluid state in a unified manner. Hence, it is necessary to establish a constitutive model that can simulate the entire process of flow liquefaction in which the soil starts from a solid phase and then transits into a fluid phase.

Unified modeling of the entire process of flow liquefaction has attracted the interest of researchers, and some pioneering work has been carried out in recent years. Sato et al. [20] proposed a fluidal-elasto-plastic model in which the whole stress of the soil is divided into three parts: the effective stress σ_{ij}^{ep}, the viscous stress σ_{ij}^{f} and the pore water pressure p. The excess pore water pressure (EPWP) ratio is used to control the phase transition process. Andrade et al. [21] proposed a combined framework that allowed the co-existence of the classical rate-independent plasticity model and Bingham model for granular media. In this framework, the solid phase begins to transit to the fluid phase when soil stress reaches the critical state line. Later, Andrade et al. [22] proposed a critical hardening modulus to detect the onset of flow liquefaction in both cyclic and monotonic loading conditions. Through similar methods, Najma and Latifi [23] proposed a flow liquefaction criterion for contractive loose sands, and proved the criterion can be applied to predict the onset of flow liquefaction in conjunction with several existing elasto-plastic models [10–12]. Prime et al. [24,25] developed a phase transition model for geomaterials and adopted the second-order work $d^2W = d\sigma_{ij}d\varepsilon_{ij}$ as the solid–fluid transition criterion. The equation $d^2W = 0$ was the demarcation point between the solid state ($d^2W > 0$) and the fluid state ($d^2W < 0$). However, in the work by Prime et al. [24], the phase transition occurs abruptly without a smooth transition process. In summary, the previous studies mainly involve two key issues: (1) when the phase transition occurs, i.e., the criterion for the phase transition; and (2) how the solid-like behavior transitions to the fluid-like behavior. Although researchers have made great progress in these two aspects, there are still some problems and challenges. First, the criteria for phase transition defined in previous studies are sometimes inconsistent with the experimental results, in which the onset of flow liquefaction occurred usually before the effective stress reaches a critical state, and the EPWP ratio is only approximately 0.5–0.7 [26,27]. Second, the mechanical characteristics of the solid-like and fluid-like behaviors are completely different, and the smooth transition from the solid-like behavior to the fluid-like behavior is not realized and remains a challenge theoretically and mathematically.

In this paper, a simple constitutive model that can associate elastoplastic and fluid constitutive relations with phase transition criteria is proposed. The elastoplastic relation is adopted to simulate the solid-like behaviors, and a fluid relation is used to simulate the fluid-like behaviors. These two kinds of models are combined by a weighting factor that is related to the EPWP ratio. Furthermore, according to the value of the phase transition criterion, two types of liquefaction behaviors, i.e., the cyclic mobility and flow liquefaction, can be distinguished automatically. If cyclic mobility occurs, only the elastoplastic relation works during the entire process of liquefaction, while if flow liquefaction occurs, the elastoplastic relation will be smoothly transited to the fluid relation.

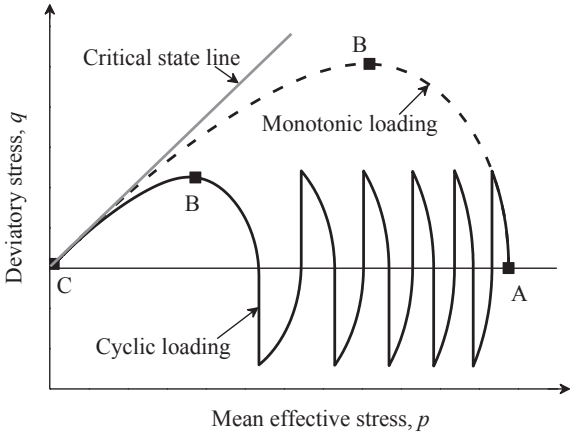

Fig. 2. Stress paths in undrained cyclic and monotonic triaxial tests on loose sand.

2. Stages of flow liquefaction

Before providing the detailed formulation of the proposed constitutive model, the entire process of flow liquefaction was examined first. The solid line in Fig. 2 illustrates the stress path in an undrained cyclic triaxial test on a loose sand sample. Point A is the initial state before loading. After the cyclic loading is applied, the effective stress of soil will decrease gradually due to the accumulation of EPWP. When the stress state reaches Point B, which is called as an instability state by researchers [28,29], the sample starts to transition from the solid phase to a fluid phase. The determination of Point B is the most crucial part in this study, which will be described in Section 3. After passing through Point B, the effective stress continues to decrease, and the sample behaves increasingly similar to a fluid. Finally, the effective stress path will reach the zero-stress state at Point C, after which the soil will lose its shear strength and stiffness completely and behave similar to a fluid.

From the above description, the process of flow liquefaction can be divided into three stages: (1) Solid stage from Point A to Point B, in which the soil behaves similar to a solid material, and its behavior can be described by a traditional elastoplastic constitutive relation; (2) Phase transition stage from Point B to Point C, in which the deformation of the soil increases rapidly but has not caused flow liquefaction. In this stage, the soil behavior possesses both solid and fluidal characteristics and can be modeled by a combination of elastoplastic and fluid relations; and (3) Fluid stage after Point C, in which the soil behaves similar to a fluid, and its behavior can be modeled by a fluid constitutive relation. The analytical scheme of the flow liquefaction process is summarized and shown in Fig. 3.

In addition to cyclic loading, monotonic loading can also induce flow liquefaction in undrained triaxial tests, which is called static liquefaction [28,30]. A typical stress path of static liquefaction is illustrated by a dashed line in Fig. 2. Similarly, the process of static liquefaction can also be divided into three stages and can be modeled by the same scheme, as shown in Fig. 3.

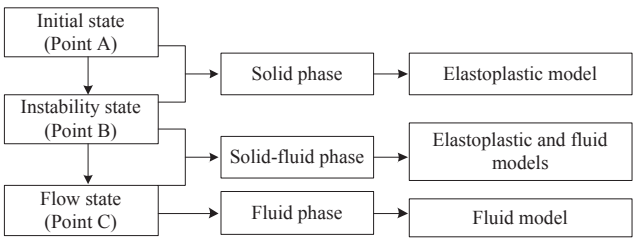

Fig. 3. Analytical scheme for flow liquefaction.

3. A constitutive model for modeling the entire process from the solid phase to full flow

3.1. Phase transition criterion

Andrade et al. [22] proposed a mathematical criterion for flow liquefaction instability based on Hill's stability theory [31]. In this study, the criterion is adopted to detect the onset of phase transition from a solid to a fluid.

According to Hill's stability theory [31], the condition for loss of stability in elastoplastic solids can be expressed as:

$$\dot{\boldsymbol{\sigma}}\cdot\dot{\boldsymbol{\varepsilon}} = 0 \tag{1}$$

where $\dot{\boldsymbol{\sigma}}$ and $\dot{\boldsymbol{\varepsilon}}$ are the stress rate and strain rate tensors, respectively. Eq. (1) implies that instability occurs when a solid can no longer sustain a small perturbation. The instability condition for the undrained triaxial condition can be expressed as:

$$\dot{p}\cdot\dot{\varepsilon}_v + \dot{q}\cdot\dot{\varepsilon}_d = 0 \tag{2}$$

where $\dot{p} = \frac{1}{3}(\dot{\sigma}_1 + 2\dot{\sigma}_3)$ is the rate of mean effective stress; $\dot{\varepsilon}_v = \dot{\varepsilon}_1 + 2\dot{\varepsilon}_3$ is the rate of volumetric strain; $\dot{q} = \dot{\sigma}_1 - \dot{\sigma}_3$ is the deviatory stress rate and $\dot{\varepsilon}_d$ is the deviatory component of the strain rate.

In the framework of an elastoplastic model, the rate of the effective stress tensor takes the form:

$$\dot{\boldsymbol{\sigma}} = \boldsymbol{E}^{ep}\cdot\dot{\boldsymbol{\varepsilon}} \tag{3}$$

where $\boldsymbol{E}^{ep}$ is the elastoplastic stiffness tensor. In the triaxial condition, Eq. (3) can be rewritten in the following form

$$\begin{Bmatrix}\dot{p}\\ \dot{q}\end{Bmatrix} = \begin{bmatrix}C_{pp} & C_{qp}\\ C_{pq} & C_{qq}\end{bmatrix}\begin{Bmatrix}\dot{\varepsilon}_v\\ \dot{\varepsilon}_d\end{Bmatrix} \tag{4}$$

Further, under undrained conditions and assuming an incompressible fluid and a solid skeleton, the volumetric strain is constant ($\dot{\varepsilon}_v = 0$). Therefore, the rate of deviatory stress can be deduced from Eq. (4) and expressed as:

$$\dot{q} = C_{qq}\dot{\varepsilon}_d \tag{5}$$

By substituting Eq. (5) into Eq. (2), the criterion can be simplified to

$$C_{qq}\dot{\varepsilon}_d^2 = 0 \tag{6}$$

Because the deviatory strain ε_d changes in the loading process and its rate $\dot{\varepsilon}_d$ will not be zero generally, the shear component in the stiffness matrix must be zero. Therefore, the criterion for the undrained triaxial condition requires

$$C_{qq} = 0 \tag{7}$$

Eqs. (1)–(7) are the general criteria for detecting the onset of the instability state in elastoplastic solids. In this study, these criteria were applied to detect the onset of the phase transition during flow liquefaction, considering flow liquefaction can be regarded as an instability state of the soil.

It should be noted here that the instability criterion expressed by Eq. (7) is a necessary but not sufficient condition for flow liquefaction. Particularly, for medium-dense sand under undrained monotonic loading condition, the soil might exhibit an instability state at the peak point of the stress path. However, the following stress path might go upward after crossing the phase transformation line [32]. The phase transformation defines a transient state in which the change from contractive to dilative behavior occurs in the sand. Due to the dilation characteristics, no flow liquefaction will occur in the medium-dense sand. Thus, for monotonic loading, using the criterion for instability state (Eq. (7)) to detect the onset of flow liquefaction should be limited to the stress paths which show pure contractive condition.

For cyclic loading conditions, using Eq. (7) to detect the onset of flow liquefaction will not cause problems because the occurrence of instability state during cyclic loading will definitely lead to flow

liquefaction. On the other hand, if flow liquefaction does not occur, the soil will not exhibit the instability sate during cyclic loading [22,33].

3.2. Combination of a solid and a fluid constitutive relation

As previously described, the mechanical behavior of soils can generally be expressed by the elastoplastic constitutive relation before flow liquefaction, while after flow liquefaction, the soils are known as to follow a fluid constitutive relation. Hence, to model the soil behaviors before/after liquefaction in a unified way, a new constitutive model based on both elastoplastic and fluid constitutive relations including the phase transition criterion is developed in this research. Furthermore, to realize a smooth transition from the solid phase to the fluid phase, a weighting factor is adopted to link the two different relations and take into account their different contribution ratios in the transient stage.

In the newly proposed constitutive model, it is assumed that the effective stress tensor of soil $\boldsymbol{\sigma}$ consists of two parts: the elastoplastic part $\boldsymbol{\sigma}^{ep}$ and fluid part $\boldsymbol{\sigma}^{f}$. These two components are linked by the weighting factor expressed in Eq. (8).

$$\boldsymbol{\sigma} = (1-\delta)\cdot\boldsymbol{\sigma}^{ep} + \delta\cdot\boldsymbol{\sigma}^{f} \tag{8}$$

where δ is the weighting factor and is called the transition parameter hereafter. A schematic view of the constitutive equation is shown in Fig. 4.

The phase transition parameter δ is used to control the different contribution ratios of the elastoplastic and fluid relations, and its value ranges from 0 to 1. When the soil behaves in the solid stage before liquefaction, the elastoplastic relation plays a major role and δ approximately equals 0. When the soil reaches the phase transition criterion, the fluidal relation starts to work together with the elastoplastic model, and the value of δ varies between 0 and 1. When the soil is completely liquefied (flow liquefaction), in which the EPWP ratio u/σ_{m0} reaches 1, the soil behaves similar to a fluid, and δ equals 1. According to these requirements, the following evolution function for δ was adopted and shown as Eq. (9).

$$\delta = 1 + \tanh A\cdot\left(\frac{u}{\sigma_{m0}}-1\right) \tag{9}$$

where u is the EPWP, σ_{m0} is the initial mean effective stress and A is a parameter that controls the shape of the variation curve of δ with u/σ_{m0}. The function is a working hypothesis used to reflect the behavior of flow liquefaction. It was first proposed by Sato et al. [34] and is slightly modified here for simplicity.

According to Eq. (9), Fig. 5 presents the relationship between δ and u/σ_{m0} at different values of A. For each curve in Fig. 5, δ approximately equals 0 in the initial stage when the value of u/σ_{m0} is small, indicating that the elastoplastic relation plays the leading role during this stage. After reaching the phase transition, Point B, the value of δ increases rapidly, indicating that the fluid relation begins to play an increasingly significant role. When u/σ_{m0} equals 1, the curves end at δ equals 1, indicating that the fluid relation plays the leading role after the soil has completely liquefied. The position of Point B varies with different values of parameter A. Therefore, in the numerical simulation, Point B can be first determined according to the phase transition criterion

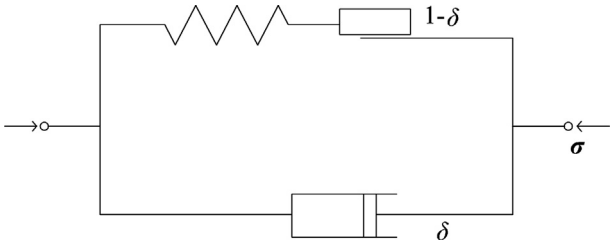

Fig. 4. Schematic view of the proposed constitutive model.

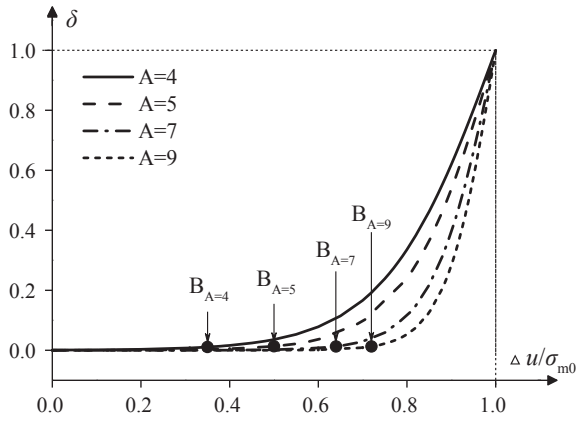

Fig. 5. Relationship between transition parameter δ and u/σ_{m0}.

introduced in the previous section, and then the value of A can be determined accordingly.

The scheme of this unified model is very simple and is suitable for any selected elastoplastic and fluid constitutive relations. In this study, two specific relations have been selected, which are introduced in the next two sections.

3.3. Elastoplastic constitutive relation

The authors of this paper have proposed an elastoplastic constitutive model describes the liquefaction behaviors of sand during the solid stage [13,35]. This model was selected as the elastoplastic relation in this study, keeping in mind that any other model could be used with the same approach. The distinct characteristic of the model is that it can describe the different undrained cyclic behaviors of sand with different densities, i.e., loose sand will fail towards the zero-effective stress state, which can trigger flow liquefaction (Fig. 1(b)); medium-dense sand will enter cyclic mobility (Fig. 1(a)), and dense sand will not liquefy at all. It will be shown later that this characteristic can be inherited in the new constitutive model. Here, a brief introduction of the elastoplastic relation is presented, and more details can be found in Zhang et al. [13] and Ye et al. [35].

The elastoplastic model is developed within the framework of critical state soil mechanics and is based on the concepts of stress-induced anisotropy [36], subloading [37] and superloading [38]. A brief description of the yield surfaces is presented as Fig. 6. The similarity ratios of the superloading surfaces to the normal yield surface, R^*, and the superloading surface to the subloading surface, R, are given as:

$$R^* = \frac{\widehat{p}}{\overline{p}} = \frac{\widehat{q}}{\overline{q}}, \quad 0 < R^* \leqslant 1 \text{ and } \frac{\widehat{q}}{\widehat{p}} = \frac{\overline{q}}{\overline{p}} \tag{10}$$

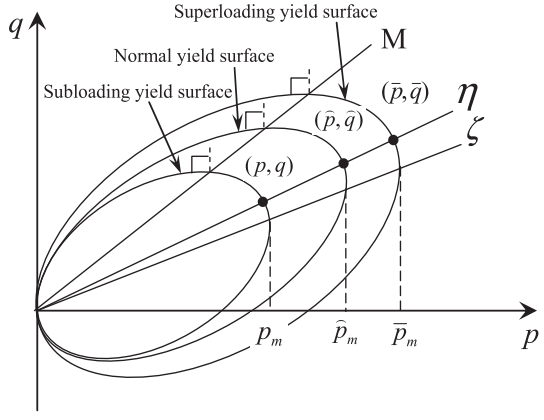

Fig. 6. Subloading, normal and superloading the yield surfaces in the p-q plane.

$$R = \frac{p}{\overline{p}} = \frac{q}{\overline{q}}, \quad 0 < R \leqslant 1, \quad and \ \frac{\overline{q}}{\overline{p}} = \frac{\widehat{q}}{\widehat{p}} = \frac{q}{p} \tag{11}$$

where $(p,\ q)$, $(\widehat{p}\ ,\ \widehat{q}\ )$ *and* $(\overline{p}\ ,\ \overline{q})$ represent the present stress state, the corresponding normally consolidated stress state and the structured stress state on the *p*-*q* plane, respectively. The present stress state is always situated on the subloading surface, which is given in the following form:

$$f = \ln\frac{p}{p_0} + \ln\frac{M^2-\zeta^2+\eta^{*2}}{M^2-\zeta^2} + \ln R^* - \ln R - \frac{\varepsilon_v^p}{C_p} = 0 \tag{12}$$

In Eq. (12), $p = \frac{1}{3}tr\boldsymbol{\sigma}$ is the mean effective stress and $p_0 = 98$ kPa is a reference stress. $\zeta = \sqrt{\frac{3}{2}\boldsymbol{\beta}\cdot\boldsymbol{\beta}}$ is an anisotropic state variable with $\boldsymbol{\beta}$ as the anisotropic stress tensor. $\eta^* = \sqrt{\frac{3}{2}\hat{\boldsymbol{\eta}}\cdot\hat{\boldsymbol{\eta}}}$ represents the difference between the stress ratio tensor $\boldsymbol{\eta}$ and the anisotropic stress tensor $\boldsymbol{\beta}$, in which

$$\hat{\boldsymbol{\eta}} = \boldsymbol{\eta}-\boldsymbol{\beta}, \ \ \boldsymbol{\eta} = \frac{\boldsymbol{S}}{p}, \ \ \boldsymbol{S} = \boldsymbol{\sigma}-p\boldsymbol{\delta}, \tag{13}$$

where $\boldsymbol{S}$ is the deviatory stress tensor and $\boldsymbol{\delta}$ is Kronecker delta tensor. In Eq. (12), C_p is expressed as:

$$C_p = \frac{\lambda-k}{1+e_0} \tag{14}$$

where λ and κ represent the compression and swelling index, respectively.

An associated flow rule is employed in the model, namely:

$$\dot{\boldsymbol{\varepsilon}}^p = \Lambda\frac{\partial f}{\partial\boldsymbol{\sigma}} \tag{15}$$

The consistency equation for the subloading yield surface can then be given as:

$$\dot{f} = 0 \Rightarrow \frac{\partial f}{\partial\boldsymbol{\sigma}}\cdot\dot{\boldsymbol{\sigma}} + \frac{\partial f}{\partial\boldsymbol{\beta}}\cdot\dot{\boldsymbol{\beta}} + \frac{1}{R^*}\cdot\dot{R}^* - \frac{1}{R}\cdot\dot{R} - \frac{1}{C_p}\cdot\dot{\varepsilon}_v^p = 0 \tag{16}$$

The evolution rule for the anisotropic stress tensor is defined as:

$$\dot{\boldsymbol{\beta}} = \frac{M}{C_p}b_r(M-\zeta)\dot{\varepsilon}_d^p\frac{\hat{\boldsymbol{\eta}}}{\|\hat{\boldsymbol{\eta}}\|} = \sqrt{\frac{3}{2}}\frac{M}{C_p}b_r(M-\zeta)\dot{\varepsilon}_d^p\frac{\hat{\boldsymbol{\eta}}}{\eta^*}, \tag{17}$$

where b_r is a parameter that controls the developing rate of anisotropy.

The evolution rule for the degree of structure, R^*, is defined as:

$$\dot{R}^* = U^*\dot{\varepsilon}_d^p, \ \ U^* = \frac{\alpha M}{C_p}R^*(1-R^*)\ (0 < R^* \leqslant 1), \tag{18}$$

in which a is a parameter that controls the rate of collapse of the structure during shearing.

The changing rate of overconsolidation is assumed to be controlled by two factors, namely, the plastic component of strain and the incremental anisotropy:

$$\dot{R} = U\|\dot{\varepsilon}_{ij}^p\| + R\frac{\eta}{M}\frac{\partial f}{\partial\boldsymbol{\beta}}\cdot\dot{\boldsymbol{\beta}}, \tag{19}$$

where

$$U = -\frac{mM}{C_p}\left[\frac{(p/p_0)^2}{(p/p_0)^2+1}\right]\ln R \quad (p_0 = 98.0\ \text{kPa},\ \ \text{reference stress}) \tag{20}$$

Here, m is a parameter that controls the losing rate for overconsolidation.

The plastic volumetric strain rate can be evaluated as:

$$\dot{\varepsilon}_v^p = \Lambda\frac{\partial f}{\partial p} = \Lambda\frac{M^2-\eta^2}{(M^2-\zeta^2+\eta^{*2})p} \tag{21}$$

If the incremental strain tensor is divided into elastic and plastic components, the elastic component is as follows:

Table 1
Parameters of the elastoplastic constitutive model.

Compression index, λ	0.05	The same as in the Cam-clay model
Swelling index, κ	0.012	
Critical state parameter, M	1.00	
Void ratio, e_N (p = 98 kPa on normal consolidation line)	0.98	
Poisson's ratio, ν	0.30	
Degradation parameter of the overconsolidation state, m	0.10	
Degradation parameter of the structure, a	1.30	
Evolution parameter of anisotropy, b_r	2.00	

$$\dot{\boldsymbol{\sigma}} = \boldsymbol{E}\cdot\dot{\boldsymbol{\varepsilon}}^e = \boldsymbol{E}\cdot(\dot{\boldsymbol{\varepsilon}}-\dot{\boldsymbol{\varepsilon}}^p) = \boldsymbol{E}\cdot\dot{\boldsymbol{\varepsilon}}-\Lambda\boldsymbol{E}\cdot\frac{\partial f}{\partial\boldsymbol{\sigma}} \tag{22}$$

Therefore, by substituting Eqs. (17), (18), (19), (21) and (22) into Eq. (16), the positive variable Λ can be rewritten as:

$$\Lambda = \frac{\frac{\partial f}{\partial\boldsymbol{\sigma}}\cdot\boldsymbol{E}\cdot\dot{\boldsymbol{\varepsilon}}}{H + \frac{\partial f}{\partial\boldsymbol{\sigma}}\cdot\boldsymbol{E}\cdot\frac{\partial f}{\partial\boldsymbol{\sigma}}} \tag{23}$$

where H is the hardening modulus and is expressed as:

$$H = \frac{1}{C_p(M^2-\zeta^2+\eta^{*2})\sigma_m}(M_s^2-\eta^2) \tag{24}$$

$$M_s^2 = M^2 - \frac{mM\ln R}{R}\left[\frac{(p/p_0)^2}{(p/p_0)^2+1}\right]\sqrt{6\eta^{*2}+\frac{1}{3}(M^2-\eta^2)^2} - 2aM(1-R^*)\eta^* + \left(1-\frac{\eta}{M}\right)\frac{\sqrt{6}Mb_r(M-\zeta)\eta^{*2}(2M^2-3\eta_{ij}\beta_{ij})}{(M^2-\zeta^2+\eta^{*2})(M^2-\zeta^2)} \tag{25}$$

Eqs. (10)–(25) are the basic equations of the elastoplastic constitutive model. As shown in Table 1, the model only employs eight parameters, among which five parameters are the same as those used in the Cam-clay model.

3.4. Fluid constitutive relation

The post-liquefaction may cause a large flow deformation; thus, some researchers regarded post-liquefied soil as fluid material to study its behavior. Kawakami et al. [39], Uzuoka et al. [15], Huang et al. [18] indicated that the behavior of a liquefied soil is similar to a Bingham fluid. Therefore, the Bingham fluid model was selected as the fluid constitutive relation in this study.

A Bingham fluid is one of the viscoplastic models in consideration of the minimum undrained strength. In a pure shear condition, the relation is expressed as:

$$\begin{aligned} &\tau = \tau_0\cdot sgn(\dot{\gamma}) + \mu\cdot\dot{\gamma}, \quad \dot{\gamma} \neq 0 \\ &\tau \leqslant \tau_0, \quad \dot{\gamma} = 0 \end{aligned} \tag{26}$$

where τ_0 is the minimum undrained strength, μ is the viscosity coefficient and $\dot{\gamma}$ is the shear strain rate.

Compared to other fluid models, the most important feature of the Bingham model is that if the initial driving shear stress is greater than the minimum undrained strength, then flow failure can occur. The schematic constitutive relation of the Bingham model is shown in Fig. 7.

3.5. Application of the phase transition criterion

In Section 3.1, the phase transition criterion for the undrained triaxial condition has been derived, as shown in Eq. (7). This criterion can be applied to the elastoplastic relation introduced in Section 3.2 to obtain a simpler form. By substituting Eq. (23) into Eq. (22), the following equation can be obtained:

$$\boldsymbol{\sigma} = \boldsymbol{E}\cdot\boldsymbol{\varepsilon}-\Lambda\boldsymbol{E}\cdot\frac{\partial f}{\partial\boldsymbol{\sigma}} = (\boldsymbol{E}-\boldsymbol{E}^p)\cdot\boldsymbol{\varepsilon} = \boldsymbol{E}^{ep}\cdot\boldsymbol{\varepsilon} \tag{27}$$

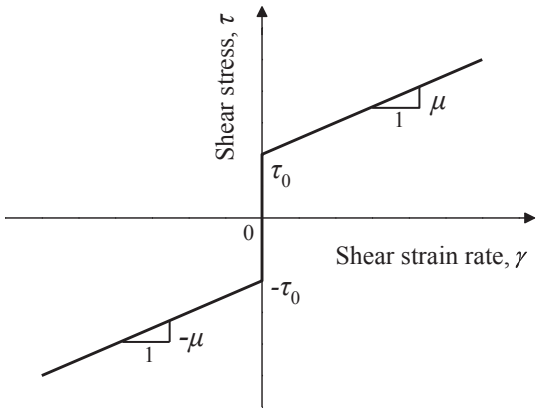

Fig. 7. Schematic constitutive relation of the Bingham model.

In a triaxial condition, $\boldsymbol{E}^p$ can be derived as

$$\boldsymbol{E}^p = \frac{\boldsymbol{E}\cdot\frac{\partial f}{\partial \boldsymbol{\sigma}}\cdot\left(\frac{\partial f}{\partial \boldsymbol{\sigma}}\right)^{-1}\cdot\boldsymbol{E}}{\frac{\partial f}{\partial \boldsymbol{\sigma}}\cdot\boldsymbol{E}\cdot\frac{\partial f}{\partial \boldsymbol{\sigma}}+H} = \frac{\begin{bmatrix} K^2\left(\frac{\partial f}{\partial p}\right)^2 & 2KG\frac{\partial f}{\partial p}\frac{\partial f}{\partial q} \\ 2KG\frac{\partial f}{\partial p}\frac{\partial f}{\partial q} & 4G^2\left(\frac{\partial f}{\partial q}\right)^2 \end{bmatrix}}{\frac{\partial f}{\partial \boldsymbol{\sigma}}\cdot\boldsymbol{E}\cdot\frac{\partial f}{\partial \boldsymbol{\sigma}}+H} \tag{28}$$

where K and G are the elastic bulk and shear modulus, respectively.

Thus, the elastoplastic stiffness tensor is obtained as:

$$\boldsymbol{E}^{ep} = \boldsymbol{E}-\boldsymbol{E}^p = \begin{bmatrix} K & 0 \\ 0 & 2G \end{bmatrix} - \frac{\begin{bmatrix} K^2\left(\frac{\partial f}{\partial p}\right)^2 & 2KG\frac{\partial f}{\partial p}\frac{\partial f}{\partial q} \\ 2KG\frac{\partial f}{\partial p}\frac{\partial f}{\partial q} & 4G^2\left(\frac{\partial f}{\partial q}\right)^2 \end{bmatrix}}{\frac{\partial f}{\partial \boldsymbol{\sigma}}\boldsymbol{E}\frac{\partial f}{\partial \boldsymbol{\sigma}}+H} = \begin{bmatrix} C_{pq} & C_{pq} \\ C_{pq} & C_{qq} \end{bmatrix} \tag{29}$$

According to Eq. (7), the phase transition criterion in an undrained triaxial condition requires that $C_{qq} = 0$. Based on Eq. (29), the hardening modulus can be deduced when $C_{qq} = 0$:

$$H_L = -\frac{1}{9}\left[\frac{M^2-\eta^2}{(M^2-\zeta^2+\eta^{*2})p}\right]^2 \tag{30}$$

H_L is a critical value of the hardening modulus at which the phase transition criterion can be satisfied, i.e., when the hardening modulus H equals H_L, where a state of instability will be triggered, and the soil begins to transit from a solid state to a fluid state.

To verify the validity of the phase transition criterion, numerical simulations for dense, medium-dense, and loose sands subjected to undrained cyclic triaxial loading were carried out using the elastoplastic constitutive model. The material parameters of the sand are shown in Table 1. The initial state parameters for each sand are shown in Table 2. This set of parameters have been adopted by the authors to simulate the behaviors of Toyoura sand, which is a standard sand for geotechnical testing in Japan. Fig. 8 illustrates the stress paths and the values of H-H_L of each sand during cyclic loading. It is shown that for dense sand, which does not liquefy, and medium-dense sand, which liquefies with cyclic mobility, the values of H-H_L are always greater than 0. These results suggest that for dense and medium-dense sand, a phase transition cannot be triggered, and flow liquefaction will not occur. While for loose sand, the value of H-H_L equals 0 at Point B, indicating that a phase transition is triggered, and the sand begins to transit from a solid to a fluid from Point B onwards. It is noticeable in Fig. 8(c) that Point B is located below the critical state line, which means that the phase transition occurred before the soil reaches the critical state. This phenomenon is consistent with the experimental results obtained by Yamamuro and Covert [26] and Yang and Pan [27]. The above simulation results proved that the proposed phase transition criterion is suitable for identifying the starting point of the phase transition in flow liquefaction.

Table 2
Initial state parameters of the elastoplastic constitutive model.

Densities	Initial void ratio, e_0	Initial degree of structure, R_0^*	Initial degree of over consolidation, $1/R_0$	Initial anisotropy, ξ_0
Dense sand	0.879	0.434	7.60	0
Medium-dense sand	0.920	0.241	4.79	0
Loose sand	1.090	0.0095	1.19	0

4. Performance of the proposed unified model

Using the new proposed constitutive model, simulations of undrained cyclic and static triaxial tests on loose sand were performed. The parameters for the elastoplastic relation are the same as shown in Tables 1 and 2. For the Bingham relation, two parameters, namely, the minimum undrained strength τ_0 and the viscosity coefficient μ, should be determined. Some researchers [24,40,41] have measured these two parameters of liquefied soil. In their studies, the values of μ range from 50 to 1000 Pa·s, and the τ_0 values range from 0.1 to 5 kPa, depending on the soil characteristics. In this simulation, $\mu = 100$ Pa·s and $\tau_0 = 3$ kPa are set for the Bingham relation. The parameter A in Eq. (9) is loading history dependent, i.e., it is not predetermined before the analysis. The phase transition criterion was first applied to determine the phase transition point, and then the value of A was determined by fitting the transition curve (Fig. 5). By this method, the value of A was determined as 8.0 in this simulation. The cyclic and static loadings started from an isotropic stress state of 296 kPa, and then the axial loading was applied with the confining pressure kept constant. The loading process was strain controlled with a loading speed of $\dot{\varepsilon}_a = 0.0001$/s. For cyclic loading, the stress amplitude was set at 60 kPa.

Fig. 9 displays the simulated results of the untrained cyclic triaxial tests. The time histories of the deviatory stress q and the EPWP ratio are shown in Fig. 9(a) and (b), respectively, and the stress-strain relationship is shown in Fig. 9(c). The solid line in Fig. 9(a) represents the whole deviatory stress of the soil, which is composed of solid stress and fluid stress according to Eq. (8). The solid and fluid stress components are also plotted by a dashed line and a dotted line, respectively. It is shown in Fig. 9 that the entire process can be divided into three stages, i.e., the solid stage, phase transition stage, and fluid stage. In the solid stage, the fluid stress component remains zero, and the whole stress is mainly contributed by the solid stress. Hence, the stress and strain of the soil develop in a traditional elastoplastic manner. When the phase transition criterion is satisfied, the instability of the soil is triggered, and the soil begins to enter the phase transition stage. During this stage, the elastoplastic stress decreases rapidly, and the fluid stress begins to increase gradually, indicating that the soil properties change from solid-like to fluid-like smoothly. When the EPWP ratio equals 1, the soil begins to enter the fluid stage. During this stage, the contribution of the solid phase vanishes, and the fluid phase plays a leading role, which implies the occurrence of flow liquefaction.

Fig. 10 displays the simulated results of the undrained monotonic triaxial test. Similarly, the entire process of static liquefaction can also be divided into three stages. The elastoplastic relation plays a leading role in the solid stage, and the Bingham relation plays a leading role in the fluid stage. In the phase transition stage, the two relations work together to determine the soil behaviors.

From the above results, it is proved that the proposed constitutive model can capture the main characteristics of soil behaviors during the entire process from the solid phase to full flow due to flow liquefaction. To verify the accuracy of the model, another simulation was conducted to reproduce the experimental results obtained by Yang and Pan [27].

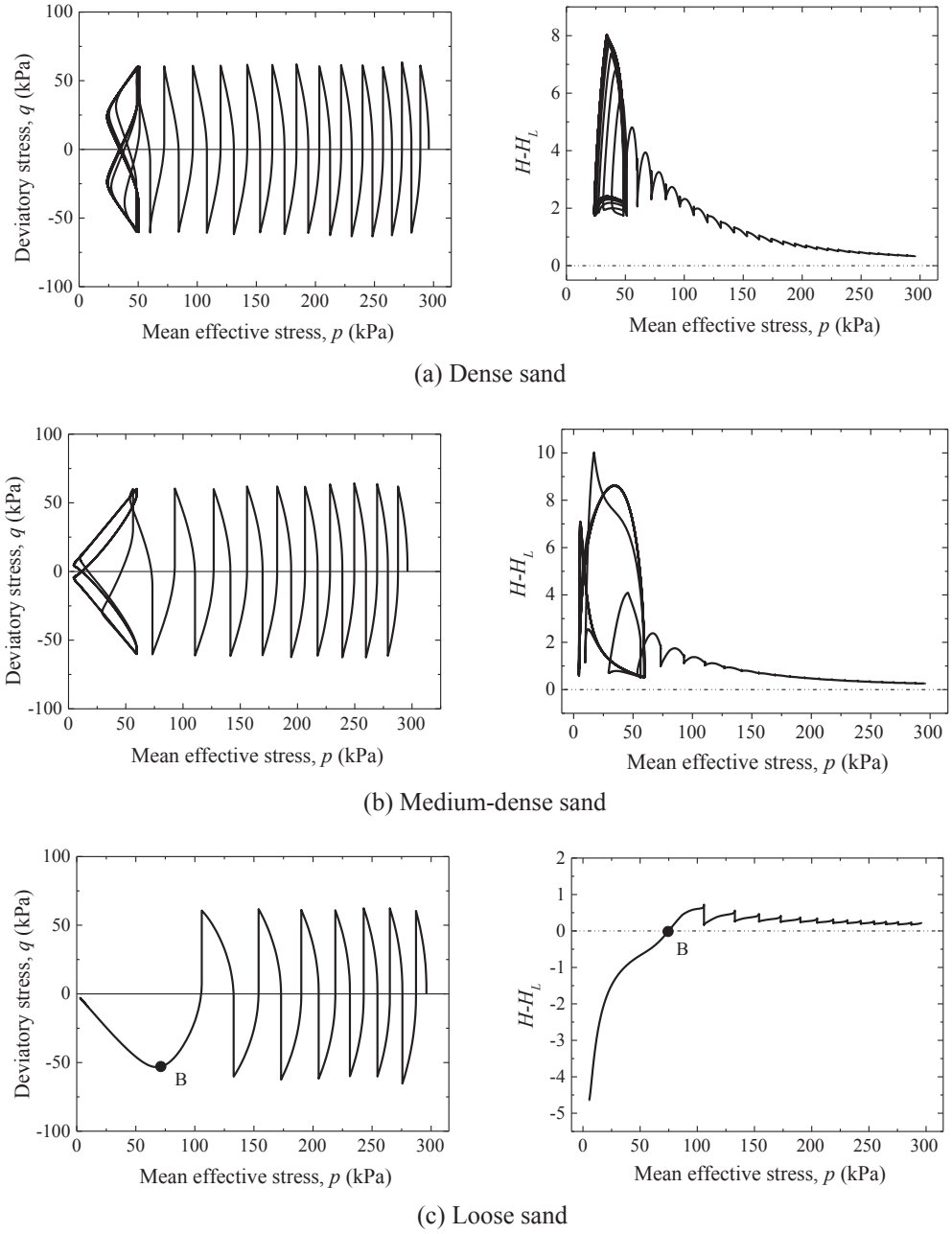

Fig. 8. Simulated responses of sands with different densities subjected to undrained cyclic triaxial loading.

They recently reported an experimental study on the flow deformation of liquefied soil using cyclic triaxial tests, and the testing results of stress path and stress-strain relationship are displayed in Fig. 11(a). The corresponding simulated results are shown in Fig. 11(b). The constitutive parameters are the same as listed in Tables 1 and 2 because the testing material in Yang and Pan's study [27] is also Toyoura sand. Note that in the experiment, the axial train can only be extended to approximately 9% due to the limitation of triaxial apparatus, while the simulated axial strain is unlimited due to the adoption of the Bingham fluid relation to simulate the post-liquefaction behavior of soil. However, in this limited range of axial strain, the simulated results agree well with the testing results, partially proving the accuracy of the proposed constitutive model.

5. Influence of minimum undrained strength τ_0 and viscosity coefficient μ

In the above constitutive model, the fluid-like behaviors of soil were modeled by the Bingham relation, in which the minimum undrained strength τ_0 and the viscosity coefficient μ are two essential parameters. To investigate the influences and sensitiveness of these two parameters, another set of simulations of undrained cyclic triaxial tests were conducted using different values of μ and τ_0, keeping the values of the other parameters the same as those above (Tables 1 and 2).

Fig. 12 displays the simulated results of the time histories of the deviatory stress q, with the same parametric value of $\mu = 100$ Pa·s but different values of τ_0. The loading speed is set the same as the above simulations with $\dot{\varepsilon}_a = 0.0001$/s. It can be seen that with the increase in τ_0 value, the deviatory stress q decreases more slowly when entering the phase transition stage, and finally maintains a larger value after entering the fluid stage.

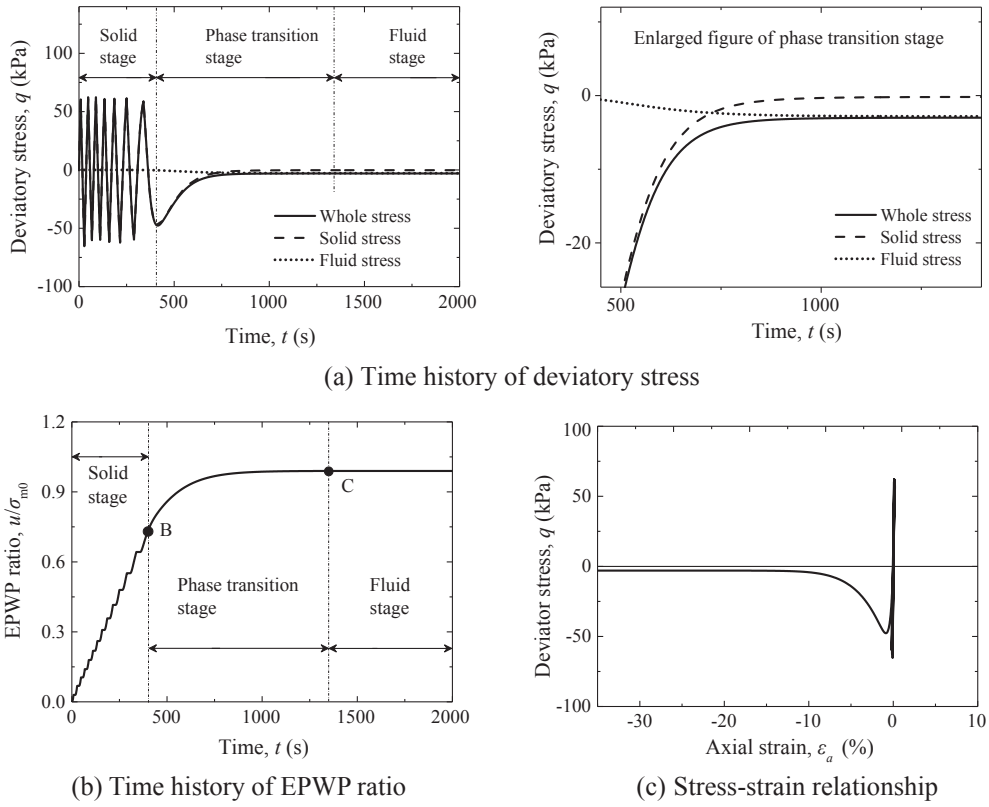

Fig. 9. Simulated behaviors of flow liquefaction during undrained cyclic triaxial testing.

Fig. 13 displays the simulated results with the same value of τ_0 but different values of μ. It is shown that the time histories of deviatory stress q are almost the same when μ varies from 100 Pa·s to 1000 Pa·s. indicating that the influence of μ is very small. However, as shown in Eq. (26), the effect of viscosity is associated with the strain speed. Fig. 14 displays the results of another set of simulations with a faster loading speed of $\dot{\varepsilon}_a = 0.1$/s. It can be seen that the influence of μ becomes more obvious and a larger value of μ will lead to a larger deviatory stress after entering the fluid stage. However, the difference between the simulated results shown in Fig. 14 is still not significant, which means that the simulated flowing behaviors of soil are not sensitive to the value of μ.

6. Discussion

In this study, a simple method was proposed to model the soil behaviors before/after flow liquefaction in a unified way, with particular attention to the phase transition process. Though its validity is proved, there remain some important issues that need to be further investigated.

First, the shearing strength and the stiffness of the liquefied soil might recover due to the dissipation of EPWP. Hence, besides the transition from a solid to a fluid phase, a reverse-phase transition process from a fluid to a solid also exists, which has not been considered in this preliminary study.

Second, to predict the flow failure of a realistic ground in engineering, the constitutive model must be incorporated into a numerical method. The suitable numerical method must be able to describe both the solid and fluid phases that may coexist in the transient state. This is a challenging problem because the numerical methods in elastoplastic mechanics are generally established based on an updated Lagrangian formulation, while a Eulerian formulation is generally used in computed fluid dynamics. These two formulations are essentially different, and their coexistence is difficult in the same transient state. A great amount of effort has been carried out in recent years to produce more

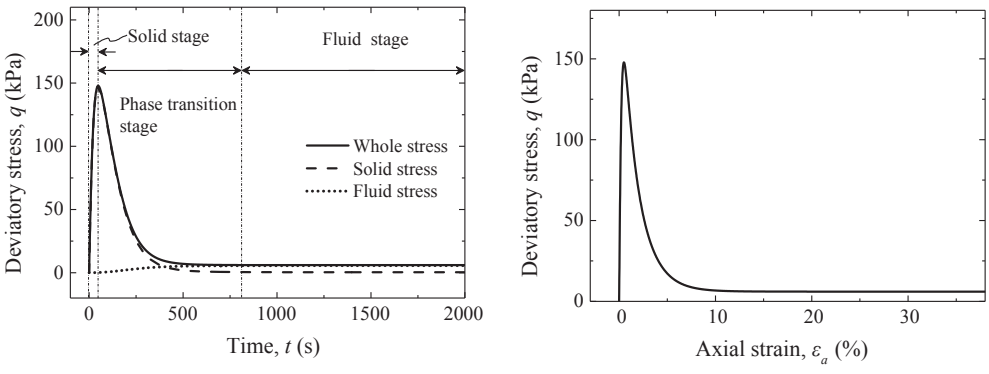

Fig. 10. Simulated behaviors of flow liquefaction during undrained monotonic triaxial testing.

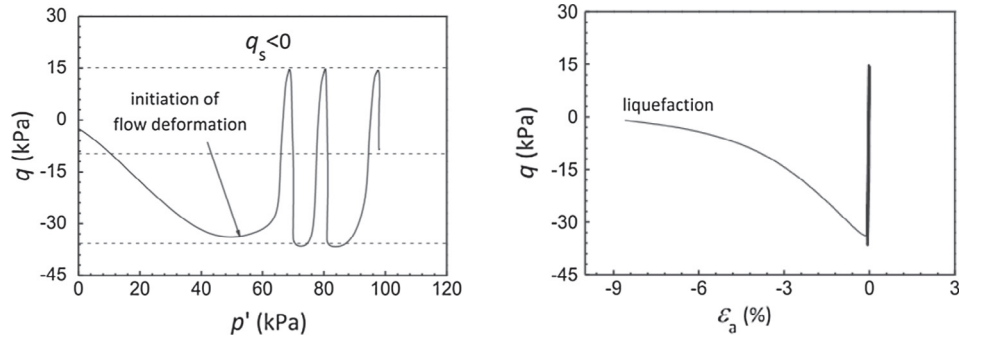

(a) Experimental results [27]

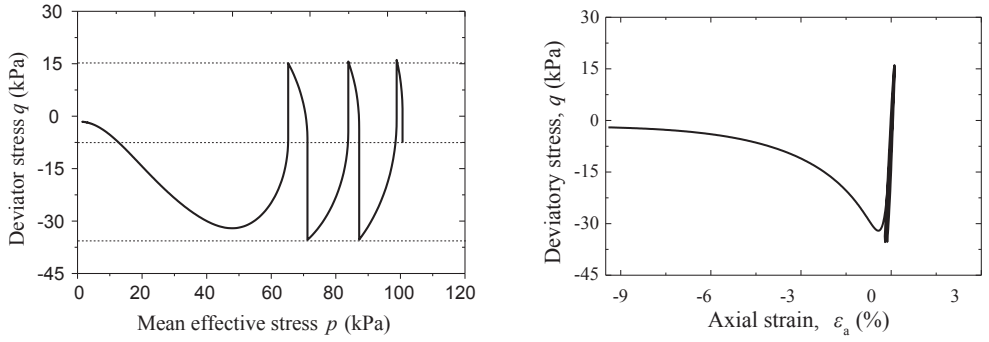

(b) Simulated results

Fig. 11. Comparison of experimental and simulated results.

versatile numerical methods, for example, the smooth particle hydrodynamics (SPH) method. The SPH method is a mesh-free method based on a pure Lagrangian formulation, which is applicable for both fluid and elastoplastic geomaterials [18,25,42,43]. The authors of this paper are trying to implement the SPH method into the analysis of the entire process of flow liquefaction, and the related research is currently underway.

7. Conclusions

This paper presents a preliminary study regarding the unified modeling of soil behaviors before/after flow liquefaction. The main conclusions of this study are as follows:

(1) The entire process from a solid phase to a fluid phase in flow liquefaction can be divided into three stages, i.e., the solid stage, the phase transient stage, and the fluid stage. In the solid stage, the soil behaves in an elastoplastic manner; in the fluid stage, the soil exhibits fluid-like behaviors; and in the phase transient stage, the characteristics of soil behavior changes from solid-like to fluid-like gradually.

(2) A phase transition criterion based on Hill's stability theory [31] was proposed to detect the onset of flow liquefaction. The application of the criterion exhibits that only loose sand can trigger a phase transition under undrained monotonic and cyclic triaxial loading conditions, indicating that flow liquefaction only occurs in loose sand. For medium-dense sand and dense sand, the phase transition criterion will not be satisfied under the same loading condition.

(3) The proposed constitutive model allows the co-existence of an elastoplastic relation and a fluidal relation during the transient stage to simulate the entire process of flow liquefaction. The elastoplastic relation plays a leading role in the solid stage and so does the fluid relation in the fluid stage. In the phase transition stage, two kinds of relations work together to determine soil behavior. The two types of relations are combined by a weighting factor, which determines the contribution ratio of the different relations.

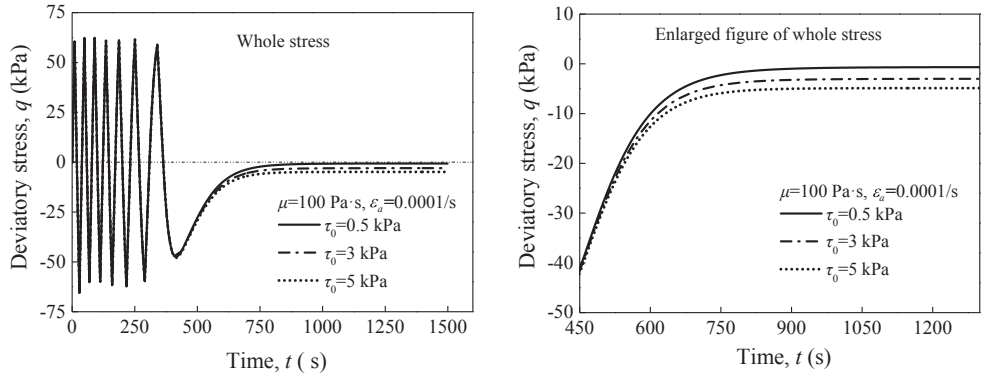

Fig. 12. Simulated behaviors of flow liquefaction with different values of τ_0.

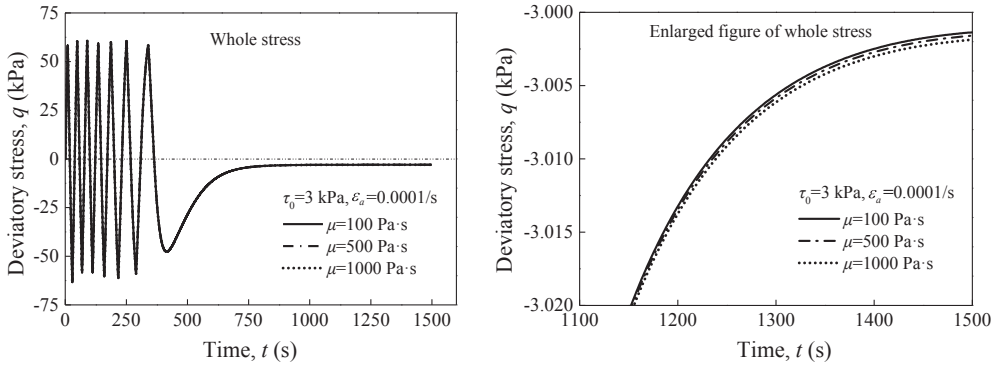

Fig. 13. Simulated behaviors of flow liquefaction with different values of μ ($\dot{\varepsilon}_a$ = 0.0001/s).

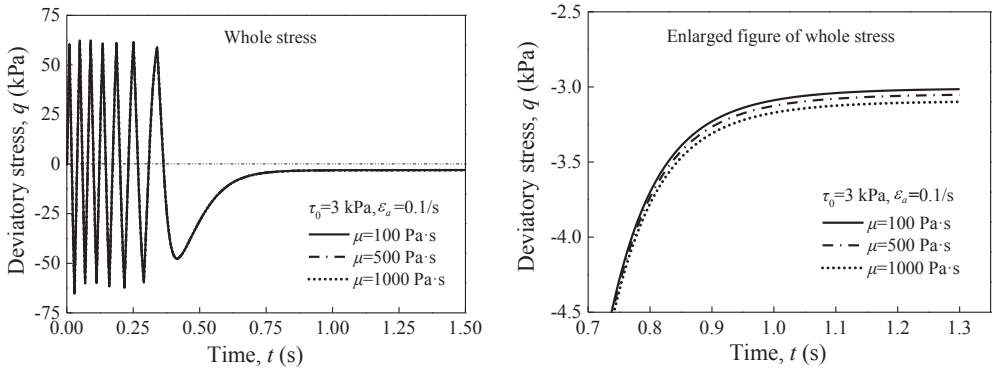

Fig. 14. Simulated behaviors of flow liquefaction with different values of μ ($\dot{\varepsilon}_a$ = 0.1/s).

(4) The scheme of the proposed model can be implemented by choosing any appropriate elastoplastic and fluidal constitutive relations. In this study, an elastoplastic relation proposed by the authors was selected to model the solid-like behavior, and the Bingham relation was selected to model the fluid-like behavior. The simulated results of undrained cyclic and monotonic triaxial tests demonstrated that the proposed model can reflect the main characteristics of soil behavior during the entire process of flow liquefaction. Additionally, this model provides a solid foundation to the numerical analyses by which boundary value problems related to flow dynamics from a solid state to a fluid state, e.g., liquefaction-induced slope failure, can possibly be solved in a unified way.

Acknowledgements

This work was supported by the Program of Shanghai Academic/Technology Research Leader (No. 17XD1403700), the National Natural Science Foundation of China (No. 41472249), the State Key Laboratory of Geo-Hazard Prevention and Geo-Environment Protection (No. SKLGP2016K019), and the Fundamental Research Funds for Central Universities.

References

[1] Seed HB. Analysis of soil liquefaction: Niigata earthquake. ASCE J Soil Mech Found 1967;93.
[2] Fu SC, Tatsuoka F. Soil liquefaction during Haicheng and Tangshan earthquake in China; a review. Soils Found 1984;24(4):11–29.
[3] Hamada M, Wakamatsu K, Ando T. Liquefaction-induced ground deformation and its caused damage during the 1995 Hyogoken-Nanbu earthquake. Terremotos 1995;1996:137–52.
[4] Huang Y, Jiang X. Field-observed phenomena of seismic liquefaction and subsidence during the 2008 Wenchuan earthquake in china. Nat Hazards 2010;54(3):839–50.
[5] Casagrande A. Liquefaction and cyclic deformation of sands-a critical review. In: 5th Pan American conference on soil mechanics and foundation engineering. Buenos Aires, Argentina; 1975.
[6] Li XS, Ming HY, Cai ZY. Constitutive modeling of flow liquefaction and cyclic mobility. Geo-Denver 2000:81–98.
[7] Zhang JM, Wang G. Large post-liquefaction deformation of sand, Part I: physical mechanism, constitutive description and numerical algorithm. Acta Geotech 2012;7(2):69–113.
[8] Zhang JM, Shamoto Y, Tokimatsu K. Cyclic critical stress states of sand with non-frictional effects. J Eng Mech 1999;125(10):1106–14.
[9] Li XS, Ming HY. Unified modeling of flow liquefaction and cyclic mobility. Soil Dyn Earthq Eng 2000;19(5):363–9.
[10] Elgamal A, Yang Z, Parra E. Computational modeling of cyclic mobility and post-liquefaction site response. Soil Dyn Earthq Eng 2002;22(4):259–71.
[11] Dafalias YF, Manzari MT. Simple plasticity sand model accounting for fabric change effects. J Eng Mech 2004;130(6):622–34.
[12] Wang R, Zhang JM, Wang G. A unified plasticity model for large post-liquefaction shear deformation of sand. Comput Geotech 2014;59:54–66.
[13] Zhang F, Ye B, Noda T, Nakano M, Nakai K. Explanation of cyclic mobility of soils: approach by stress-induced anisotropy. Soils Found 2007;47(4):635–48.
[14] Kim J, Kawai T, Kazama M. Laboratory testing procedure to assess post-liquefaction deformation potential. Soils Found 2017;2017(57):905–19.
[15] Uzuoka R, Yashima A, Kawakami T, Konrad JM. Fluid dynamics based prediction of liquefaction induced lateral spreading. Comput Geotech 1998;22(3–4):243–82.
[16] Chen Y, Liu H, Wu H. Laboratory study on flow characteristics of liquefied and post-liquefied sand. Chin J Geotech Eng 2006;17(suppl. 1):s23–32.
[17] Moriguchi S. CIP-based numerical analysis for large deformation of geomaterials PhD thesis Japan: Gifu University; 2005.
[18] Huang Y, Zhang W, Mao W, Jin C. Flow analysis of liquefied soils based on smoothed particle hydrodynamics. Nat Hazards 2011;59(3):1547–60.
[19] Zhou EQ, Wang ZH, Chen GX, Cong L. Constitutive model for fluid of post-liquefied sand. Chin J Geotech Eng 2015;37(1).
[20] Sato T, Moon Y, Uzuoka R. Fluidal-elasto-plastic constitutive equation of sand and unified analysis of liquefaction and flow processes of ground. Proc JSCE 2002;717:53–64. (in Japanese).
[21] Andrade JE, Chen Q, Le PH, Avila CF, Evans TM. On the rheology of dilative granular media: bridging solid- and fluid-like behavior. J Mech Phys Solids 2012;60(6):1122–36.
[22] Andrade JE, Ramos AM, Lizcano A. Criterion for flow liquefaction instability. Acta Geotech 2013;8(5):525–35.
[23] Najma A, Latifi M. Predicting flow liquefaction, a constitutive model approach. Acta Geotech 2017;12(4):793–808.
[24] Prime N, Dufour F, Darve F. Unified model for geomaterial solid/fluid states and the transition in between. J Eng Mech 2013;140(6):682–94.
[25] Prime N, Dufour F, Darve F. Solid–fluid transition modelling in geomaterials and application to a mudflow interacting with an obstacle. Int J Numer Anal Met 2014;38(13):1341–61.
[26] Yamamuro JA, Covert KM. Monotonic and cyclic liquefaction of very loose sands

with high silt content. J Geotech Geoenviron 2001;127(4):314–24.
[27] Yang ZX, Pan K. Flow deformation and cyclic resistance of saturated loose sand considering initial static shear effect. Soil Dyn Earthq Eng 2017;92:68–78.
[28] Lade PV. Static instability and liquefaction of loose fine sandy slopes. J Geotech Eng 1992;118(1):51–71.
[29] Vaid YP, Eliadorani A. Instability and liquefaction of granular soils under undrained and partially drained states. Can Geotech J 1998;35(6):1053–62.
[30] Vaid YP, Sivathayalan S. Fundamental factors affecting liquefaction susceptibility of sands. Can Geotech J 2000;37(3):592–606.
[31] Hill R. A general theory of uniqueness and stability in elastic-plastic solids. J Mech Phys Solids 1958;6(3):236–49.
[32] Ishihara K. Liquefaction and flow failure during earthquakes. Géotechnique 1993;43(3):351–451.
[33] Mohammadnejad T, Andrade JE. Flow liquefaction instability prediction using finite elements. Acta Geotech 2015;10(1):83–100.
[34] Sato T, Moon Y, Uzuoka R. Unified analysis of liquefaction and flow processes of inclined ground using fluidal elasto-plastic model. Proc JSCE 2002;722:109–19. (in Japanese).
[35] Ye B, Ye GL, Zhang F, Yashima A. Experiment and numerical simulation of repeated liquefaction-consolidation of sand. Soils Found 2007;47(3):547–58.
[36] Sekiguchi H. Rheological characteristics of clays. In: 9th ICSMFE congress: soil mech found eng, Tokyo, Japan; 1977. p. 289–92.
[37] Hashiguchi K, Chen ZP. Elastoplastic constitutive equation of soils with the subloading surface and the rotational hardening. Int J Numer Anal Meth Geomech 1998;22(3):197–227.
[38] Asaoka A, Nakano M, Noda T. Superloading yield surface concept for highly structured soil behavior. Soils Found 2000;40(2):99–110.
[39] Kawakami T, Suemasa N, Hamada M, Sato H, Katada T. Experimental study on mechanical properties of liquefied sand. In: 5th U.S.–Japan workshop on earthquake resistant design of lifeline facilities and countermeasures against soil liquefaction. Technical report NCEER-94-0026, Salt Lake City, USA; 1994. p. 285–99.
[40] Coussot P, Proust S, Ancey C. Rheological interpretation of deposits of yield stress fluids. J Non-Newt Fluid Mech 1996;66(1):55–70.
[41] Pastor M, Merodo JAF, Herreros MI, Mira P, Gonzalez E, Haddad B, et al. Mathematical, constitutive and numerical modelling of catastrophic landslides and related phenomena. Rock Mech Rock Eng 2008;41(1):85–132.
[42] Bui HH, Sako K, Fukagawa R. Numerical simulation of soil–water interaction using smoothed particle hydrodynamics (SPH) method. J Terramechanics 2007;44(5):339–46.
[43] Huang Y, Zhang W, Dai Z, Xu Q. Numerical simulation of flow processes in liquefied soils using a soil–water-coupled smoothed particle hydrodynamics method. Nat Hazards 2013;69(1):809–27.